Journal of Reproduction and Development, Vol. 70, No 5, 2024

Original Article

Autophagy in the corpus luteum correlates with tissue growth in pregnant rats

Yasuaki OISHI[1)*], Koji ASAKAWA[1)*], Yuri ISHIWATA[1)], Shota OKA[1)], Ryota TERASHIMA[1)], Makoto SUGIYAMA[2)], Keiichiro KIZAKI[3)], Mitsumori KAWAMINAMI[1, 4)] and Shiro KURUSU[1)]

[1)]*Laboratory of Veterinary Physiology, Kitasato University School of Veterinary Medicine, Aomori 034-8628, Japan*
[2)]*Laboratory of Veterinary Anatomy, Kitasato University School of Veterinary Medicine, Aomori 034-8628, Japan*
[3)]*Laboratory of Veterinary Physiology, Cooperative Department of Veterinary Medicine, Iwate University, Iwate 020-8550, Japan*
[4)]*Laboratory of Veterinary Physiology, Okayama University of Science, Ehime 794-8555, Japan*

Abstract. The developmental activation of the corpus luteum (CL) structurally and functionally is critical for the temporally regulated establishment, maintenance, and termination of pregnancy in rats. In this study, we have investigated the possible involvement of autophagy in the regulation of the CL during pregnancy in rats. The expression ratio of microtubule-associated protein light chain 3 (LC3)-II/-I, a widely used indicator of autophagic activity, in the CL remained relatively stable until day 15 of pregnancy. Subsequently, it progressively increased until day 21, and then declined until day 3 postpartum. This fluctuation was closely associated with the tissue weight of the CL rather than progesterone (P4) production activity. Light and electron microscopy revealed the presence of immunoreactive LC3 aggregates and irregularly shaped autolysosome-like microstructures in the cytoplasm of luteal cells during late pregnancy. Notably, a bolus intrabursal injection of the autophagy inhibitor bafilomycin A1 on day 15 of pregnancy resulted in a significant reduction in luteal cell size and disrupted the normal alteration of circulating P4 levels. Consequently, treatment with this inhibitor increased the likelihood of the varied timing (both advanced and delayed) of delivery and led to reduced body weight in neonates when compared with the vehicle-treated control group. Our findings suggest that autophagy in the rat CL contributes to luteal tissue growth, influences P4 production, and thereby fine-tunes the regulation of gestation length in rats.
Key words: Autophagy, Corpus luteum, Parturition, Pregnancy, Rat

(**J. Reprod. Dev. 70:** 286–295, 2024)

The corpus luteum (CL) is a transient tissue originating from ruptured follicles after ovulation and secretes progesterone (P4), a pivotal endocrine regulator of mammalian pregnancy and parturition [1, 2]. This steroid hormone guides implantation and decidualization in early pregnancy, subsequently maintaining myometrial quiescence and suppressing the maternal immune response for embryo/fetal growth [1, 2]. In rats and mice, CL serves as the sole source of P4 throughout pregnancy, and its structural and functional activation is orchestrated by placental lactogen (PL)-I and-II, intra-luteal estradiol-17β (E2), and P4 during mid-to-late gestation [3–6]. Conversely, the timely attenuation of P4 secretion is crucial for initiating normal vaginal delivery of adequately developed fetuses. The timing of delivery is rigorously regulated, as both pre- and post-term deliveries have adverse effects on neonatal and maternal viability. Functional luteolysis, which involves a reduction in P4 secretion, triggers the parturition cascade, followed by structural luteolysis, which entails the death and elimination of luteal steroidogenic and capillary endothelial cells. The primary mode of this cell death is considered to be apoptosis [1, 2]. Other types of CL exist in non-fertile states (cycle, pseudopregnancy, and lactation) depending on the species and have diverse regulatory mechanisms governing their structure and function [1, 2].

Autophagy, originally identified as a fundamental cellular protection mechanism against various stressors, such as mild starvation [7], comprises two major processes: the formation of autophagosomes containing aberrant proteins and organelles, and the subsequent fusion of autophagosomes with lysosomes to form autolysosomes, where unwanted materials are degraded and recycled [7]. Severe stressors may lead to autophagy-dependent cell death, termed "autophagic cell death (ACD)" [7, 8]. The ACD has also been proposed to participate in CL regression [9, 10]. Extensive past studies with pseudopregnant and pregnant rats [11–14], cycling and pregnant pigs [15, 16], cycling and pregnant goats [17], and cycling cows [18] have shown increased expression of key autophagy-related molecules such as microtubule-associated protein light chain 3 (LC3)-II, beclin-1, and lysosome-associated membrane protein 1 in regressing CL. However, causality has not been proven in most studies using non-rodent animal models. Another line of evidence has revealed that autophagy is associated with rat follicular luteinization [19] and the stable but critical secretion of P4 in mid-pregnant mice [20]. The expression of beclin-1 in pig and human CL [16, 21] was positively associated with P4 secretory activity. The diverse characteristics of the CL of the species, types, states (developing, functioning, or regressing), and structural and functional indices, combined with the dual nature of autophagic function, considerably complicate the issue of how autophagy is implicated in CL regulation.

In order to reveal the possible physiological function of autophagy in the CL, we employed a pregnant rat model in which the CL under-

Received: February 27, 2024
Accepted: June 17, 2024
Advanced Epub: July 7, 2024

Correspondence: S Kurusu (e-mail: kurusu@vmas.kitasato-u.ac.jp)
* Y Oishi and K Asakawa contributed equally to this study.

went full functional and structural activation and regression during its lifespan. Our investigation began by determining the occurrence and activity of autophagy in the CL throughout gestation and the early postpartum period, correlating the findings with the structural and functional indices of the CL. Additionally, transmission electron microscopic (TEM) observation and histochemical analysis of luteal cells complement the investigation on autophagy with reference to steroidogenesis-related lipid droplets (LD) and mitochondria [22–26]. Furthermore, apoptotic activity was assessed using a representative marker, caspase 3 [27–29] to explore its possible association with autophagy in regressing CL. Finally, ovarian-specific chemical inhibition was employed to investigate whether autophagy affects luteal structure and function and whether CL autophagy influences the dam's parturition behavior and fetal and neonatal growth.

Materials and Methods

Animals and tissue sampling

All procedures were performed in accordance with the Guidelines of the Animal Care and Use Committee of Kitasato University School of Veterinary Medicine (approval number, 18-051). Female Wistar–Imamichi rats were purchased from SLC Japan (Shizuoka, Japan). Animals were housed in an air-conditioned room with controlled lighting. Rat chow and tap water were provided *ad libitum*.

Pregnant rats of 3 to 4 months old were prepared as reported previously [30, 31]. The day of fertilization (vaginal estrus smear with sperm positive) was designated as day 1 of pregnancy (PRG1 in this study). In our breeding colony, normal delivery was completed mostly by the morning of the PRG23. Tissues and blood were sampled from rats in the morning (0900–1100 h) of PRG6, 12, 15, 18, 21, and 23 and on day 3 postpartum (PP3) (n = 6–7 rats for each group). Blood samples were collected via abdominal artery or heart puncture under isoflurane anesthesia. Following euthanasia by cervical dislocation, the ovaries were harvested, and the CL of pregnancy were separated from the ovaries. For each animal, the CL was counted and tissue wet weights were measured. The average tissue weight of all of the collected CLs from two ovaries of a rat was treated as one data sample, and the data for CL weight, shown in Fig. 1B, were obtained from 5–7 rats. They were stored frozen until analyses of LC3 and caspase 3 contents. Tissue samples from PRG6, PRG15, PRG18, PRG21, and PP3 rats and rats treated with an autophagy inhibitor (bafilomycin A1, Baf A1, Sigma-Aldrich, St. Louis, MO, USA) or vehicle on PRG15 or PRG19 and sampled on PRG21 were subjected to tissue fixation for histological studies. Blood plasma was kept frozen (–20ºC) until the P4 assay.

Western blot analysis

Western blot analyses of LC3 and caspase 3 were performed as described previously [32]. The CL tissues were homogenized, sonicated, and boiled for 5 minutes in SDS sample buffer. The samples containing 20 µg of protein were electrophoresed on 10% SDS-PAGE gel (Bio-Rad, Hercules, CA, USA), and proteins were transferred onto polyvinylidene fluoride membranes (Bio-Rad). Membranes were blocked with 5% skim milk solution (FUJIFILM Wako Pure Chemical Corporation, Osaka, Japan) for 1 hour at room temperature and then incubated with primary antibodies: anti-LC3 (1:500, Cat.# NB100-2220, Novus Biologicals, Centennial, CO, USA), anti-caspase 3 (1:200, Cat.# RB-1197-P1, Thermo Scientific, Waltham, MA, USA) or anti-β-actin (1:5000, Cat. # sc-47778, Santa Cruz Biotechnology, Dallas, TX, USA) overnight at 4ºC. After washing, the membranes were then incubated with peroxidase-conjugated goat IgG fraction

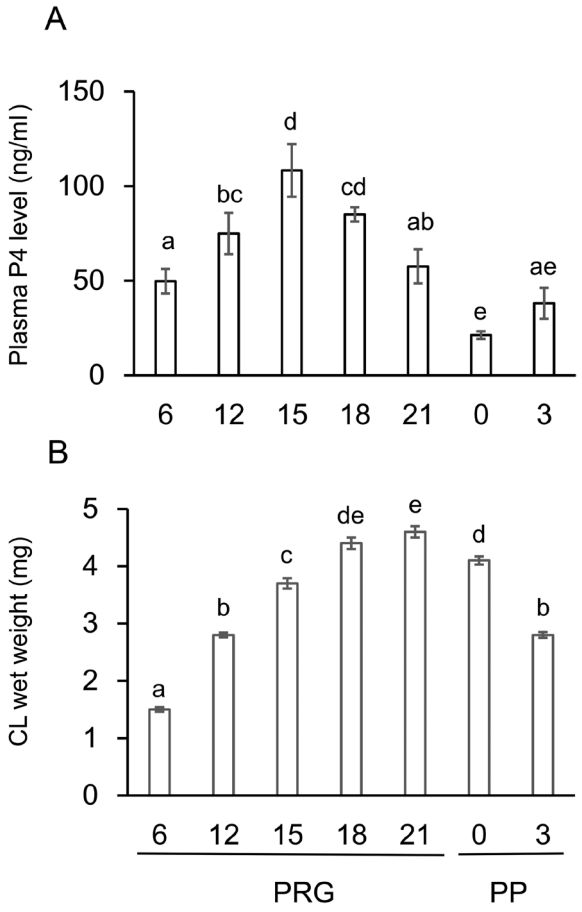

Fig. 1. Changes in the plasma P4 level and the CL weight throughout pregnancy and postpartum. P4 levels in the circulating blood plasma (A) and wet weight of the CL tissue (B) in intact rats were determined throughout pregnancy and the postpartum period. Data are presented as the mean ± SEM (n = 6, A; n = 5–7, B). Different letters in A and B indicate significant differences ($P < 0.05$).

to mouse IgG or rabbit IgG (1:50000, Code: NA934, GE Healthcare, Buckinghamshire, UK) for 2 h at room temperature. Immunoreactive proteins were detected using ECL Prime Western Blotting Reagent (GE Healthcare, Chicago, IL, USA). The signals were analyzed using an ImageQuant LAS 4000 digital imaging system (GE Healthcare).

Immunohistochemistry

Immunohistochemistry was conducted to localize LC3 and cleaved caspase 3 expression [29, 32, 33]. Ovaries were fixed in Bouin's solution overnight at 4ºC, dehydrated, and embedded in paraffin. Serial section at 4–6 µm in thickness were deparaffinized. Endogenous peroxidase activity was blocked by pre-treatment with 0.3% H_2O_2 in methanol for 30 min. Sections were incubated with an anti-LC3 antibody (1:400) (NB 100-2220, Novus Biologicals) or anti-cleaved caspase-3 antibody (1:200, Cat. # 2305-PC-020, Trevigen, Gaithersburg, MD, USA) overnight at 4°C. The former antibody failed to distinguish between LC3-I and LC3-II, and a negative control group using an antibody pre-absorbed with LC3 blocking peptide (Novus Biologicals) was prepared in order to ensure the reliability of the immunoreaction. The Vectastain Elite ABC staining kit (Vector Laboratories, Burlingame, CA, USA) was used for staining. Avidin-biotin-peroxidase complex was revealed by treatment with 3, 3′-diaminobenzidine tetrahydrochrolide followed

by hematoxylin counterstaining.

Transmission electron microscopy (TEM)

Intact ovarian tissues of PRG15, PRG21, and PP3 and those treated with Baf A1 (625 pg/rat) on PRG15 and sampled on PRG21 were fixed by immersion in Karnovsky solution (2% glutaraldehyde and 2% paraformaldehyde in 0.03 M HEPES buffer, pH 7.4). Postfixation was performed using 1% osmium tetroxide/1.5% potassium ferrocyanide [33]. The tissue samples were dehydrated and embedded in epoxy resin. Ultrathin sections were cut using Ultracut N (Reichert-Nissei, Wien, Austria), stained with uranyl acetate followed by lead citrate, and examined under a Hitachi H-7650 transmission electron microscope (Hitachi Ltd., Tokyo, Japan).

Sudan staining

Sudan III staining of the CL was performed to evaluate the neutral lipid contents supplementarilly. Intact ovarian tissues of PRG15, PRG18, PRG21 and PP0 and that treated with Baf A1 (125 pg/rat) or vehicle on PRG19 and sampled on PRG21 were fixed in 4% paraformaldehyde overnight at 4ºC followed by immersion in 30% sucrose solution overnight at 4ºC and embedded in OCT compound. Sudan staining was performed using a standard method [34]. Frozen sections (7 µm in thickness) were washed with H_2O, immersed in 1% KOH solution for 30 sec, washed with H_2O and 50% ethanol for 10 sec, and stained with Sudan III solution (FUJIFILM Wako Pure Chemical Corporation) for 90 min. The slides were washed with 50% ethanol and counterstained with hematoxylin.

Animal experiment in vivo

Given the finding of an increment in luteal autophagic activity from PRG15 through PP0, its possible roles in the CL itself and the control of pregnancy state were examined using a pharmacological approach. To limit the inhibitory action on the ovarian CL *in vivo*, the drug was injected into the ovarian bursa, as described in our previous research [32, 35, 36]. Baf A1, an inhibitor of autolysosome formation, was administered once on PRG15, and its effects on cell size and P4 secretory activity of the CL, the occurrence of dam delivery, and fetal and neonatal growth rates were determined. Rats on PRG15 under isoflurane anesthesia were subjected to lateral abdominal incisions, and the ovarian bursa was exposed. 200 µl of vehicle (5% dimethyl sulfoxide in physiological saline) or Baf A1 (62.5 or 312.5 pg/200 µl) was injected into one ovarian bursa using a syringe and repeated on the other side. No visible leakage of the injected solution or swelling of the bursa was observed. After injection, the ovaries were positioned back into the abdominal cavity, and the muscles and skin were sutured separately. To minimize the general side effect(s) of this surgical treatment and to maximize the specific effect of the reagent on the physiological status of pregnant dams, we performed this operation carefully and correctly and completed it in one dam within 20–30 min. To examine the time-dependency of the effect of Baf A1, other groups that received the inhibitor or vehicle on PRG19 were also prepared. The treated rats were kept and examined for the timing of delivery from PRG22 through PRG25, in the morning (0900 h) and the evening (1800 h) of each day. When delivery was confirmed, the number and body weight of the neonates were instantly measured. Given the significant reduction in neonatal body weight and the varied timing of delivery in Baf A1-treated rats, rats in the experimental and control groups were also prepared for the measurement of luteal growth (luteal cell size) and P4 secretion. Rats treated with the vehicle or Baf A1 at PRG19 were euthanized on PRG21, and CL tissues were evaluated morphologically. Rats treated with vehicle or Baf A1 on PRG15 were euthanized on PRG18 and PRG21. Fetal weights were determined, and CL tissues were analyzed for luteal cell size. Further experiments were conducted to investigate changes in plasma P4 levels in association with the timing of parturition in each individual. Rats receiving vehicle or Baf A1 on PRG15 had blood taken via heart puncture at 0, 24, and 72 h (approximately 0.15 ml at each sampling) after drug administration and then examined for their timing of parturition. Blood plasma was frozen for P4 measurements.

Assessment of luteal function and morphology

Functional and morphological indices of the CL were validated by the assay of circulating blood P4 levels and quantitative measurement of the cross-sectional area of luteal (steroidogenic) cells using standard histology. P4 in the plasma of intact pregnant rats and rats after treatment was extracted using n-hexane and assayed with a radioimmunoassay, as reported previously [30, 32]. The ovaries were stained with hematoxylin and eosin. Luteal cells, regardless of large and small luteal cells, were randomly selected from the CL of pregnant rats (30 cells/CL, 3 CL/rat, ≥ 3 rats in each group) and were morphometrically analyzed for cross-sectional area using Image J software.

Statistical analysis

All of the numerical values were treated statistically and presented as mean ± standard error of the mean (SEM) (sample numbers are indicated). The means of the different groups were analyzed using one-way ANOVA, followed by the Tukey-Kramer multiple comparison test. A P value less than 0.05 was considered to be statistically significant.

Results

Temporal changes in structural and functional parameters of CL during gestation and postpartum

Functional and structural indices of the CL were examined from PRG6 to PP3. Plasma P4 levels increased from PRG6, reached to a peak level (108.3 ± 13.9 ng/ml) on PRG15, kept high level, but declined gradually around PRG21 and to the nadir on PRG23 (PP0) (Fig. 1A). The wet weight of CL tissue showed 2.5-fold linear increase from PRG6 to PRG15, showed further increase and a peak on PRG21 (4.6 ± 0.1 mg) and declined very gradually on PP0 and thereafter (Fig. 1B). These dynamics were similar to those previously reported in rats of a similar strain [41, 42].

LC3 expression and localization in luteal cells

LC3-I and -II proteins were detected in the CL during pregnancy and the postpartum period (Fig. 2A). LC3-I content relative to β-actin was consistent throughout the study period. In contrast, the level of LC3-II increased progressively from PRG6, peaked at PRG21 and then declined through to PP3 (Fig. 2B). Although the LC3-II/-I ratio is less recommended than LC3-II for the level of autophagic flux [37], the ratio showed a similar temporal fluctuation that correlated with CL tissue weight rather than with P4 secretory activity (Fig. 2C). LC3 immunoreactivity (to both LC3-I and-II) was present in the CL; for example, that of PRG21 (Fig. 2D), and antibody neutralization with a blocking peptide abolished this immunoreaction (Fig. 2D). The most intense immunoreaction in whole tissue and marked aggregates in the cytoplasm of luteal cells were noted in the CL on PRG21 throughout gestation and the postpartum period. Baf A1-treated CL showed enhanced LC3 immunoreactivity (data not shown).

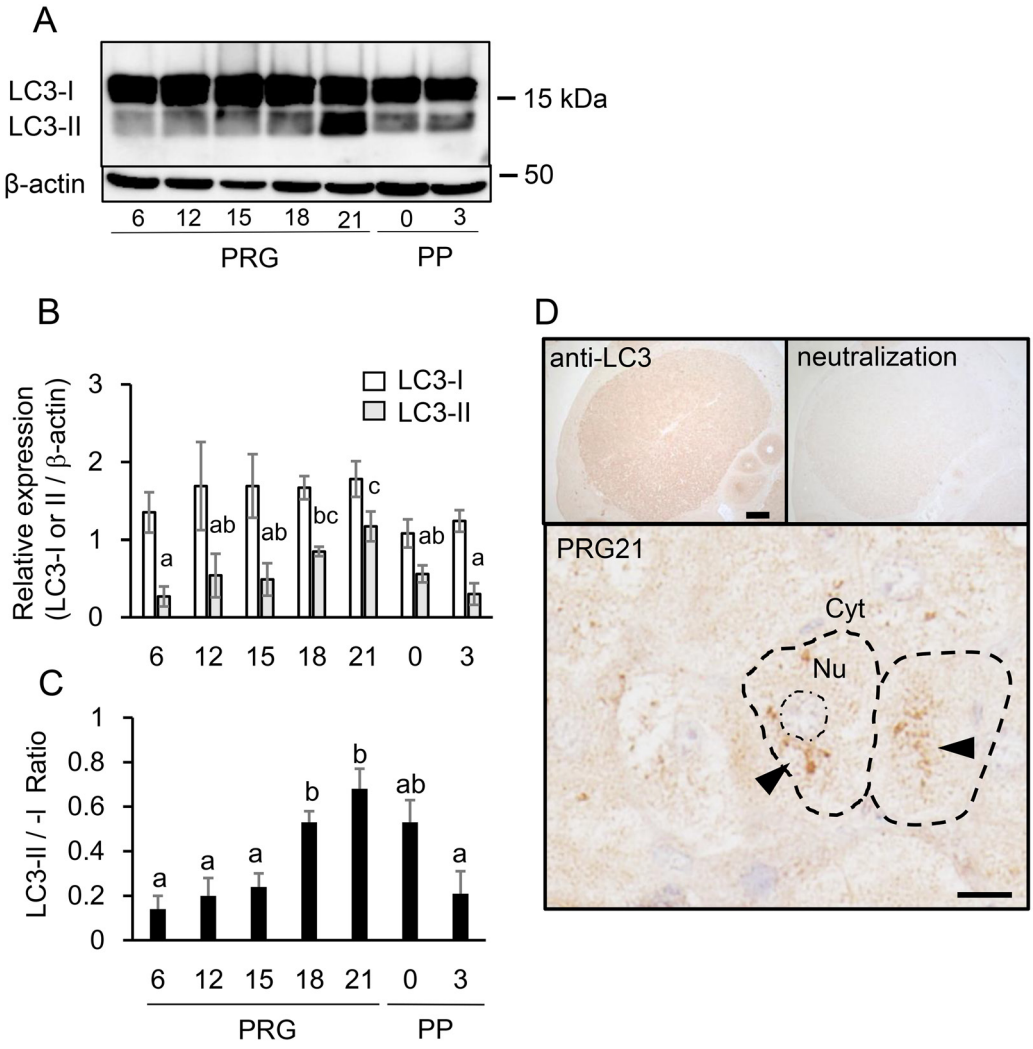

Fig. 2. Expression of LC3 proteins in CL tissue. (A) Typical immunoblots of LC3-I and -II in CL tissue throughout pregnancy and postpartum. (B) Protein expression of LC3-I and -II relative to β-actin was determined and shown (mean ± SEM, n = 6). (C) Ratio of LC3-II to -I was calculated and shown (n = 6). Different alphabetical letters in each Fig. B (LC3-II value) and C indicate significant differences ($P < 0.05$). (D) Immunohistochemical staining of LC3 (to both LC3-I and –II) in CL on PRG21. Note the loss of immunoreaction after antibody neutralization and aggregative immunostaining (black triangle) in the cytoplasm. Scale bars, 200 μm (the top left) and 20 μm (the bottom).

TEM observation and Sudan staining of luteal cells

We observed and also compared the microstructures of luteal cells on PRG15, PRG21, and PP3 (Fig. 3). Intact nuclei with mitochondria and endoplasmic reticulum (ER) were observed. Irregular shapes of voids were particularly noted in the cytoplasm on PRG15 (Figs. 3A, E), and increased both in size and number on PRG21 (Fig. 3B). At a higher magnification, they were double- and single-membranous structures (Fig. 3F), possible type(s), or processes of autophagosomes and/or autolysosomes. Another type of luteal cell with few irregular voids but developed ERs was also observed on PRG21 (Figs. 3C, G). High-density secretory granules were also observed. When compared with the relatively stable composition and abundance of microstructures in luteal cells in PRG15, a variety of microstructures were noted across luteal cells in PRG21. On PP3, the luteal cells contained remarkably large LDs (Figs. 3D, H). In rat CL treated with Baf A1, some luteal cells had fewer irregular voids and increased, small-sized LD, while other cells had abnormal mitochondrial structures, part of which were surrounded by a membranous structure (Figs. 3I, J).

Using Sudan staining, we roughly evaluated lipid contents at different ages of the CL and related them to autophagy and steroidogenic functions. Luteal cells on PRG15 contained moderate LD storage, which increased on PRG18 (Supplementary Figs. 1A, B). The LD content decreased once on PRG21 and increased again on PP0 to the level of PRG18 (Supplementary Figs. 1C, D). Baf A1 treatment, but not vehicle treatment, on PRG19 blocked partially the decreased staining in CL tissue on PRG21 (Supplementary Figs. 1E, F).

Caspase 3 expression and localization in CL

Given the finding of the concomitant increase in LC3 and cleaved caspase 3 in the aging CL of pseudopregnant rats [11], caspase 3 expression was determined in the CL of pregnant rats experiencing drastic structural and functional changes. Inactive and active forms of caspase 3, which are pro-caspase 3 and cleaved caspase 3, were detected in the CL throughout pregnancy and postpartum (Fig. 4A). The pro-caspase 3 content did not change (Fig. 4B), but the cleaved caspase 3 content tended to increase on PRG18 and PRG21 and decrease on PP0 and PP3 (Fig. 4C). Immunohistochemistry revealed that cleaved caspase 3 expression in luteal cells was enhanced on

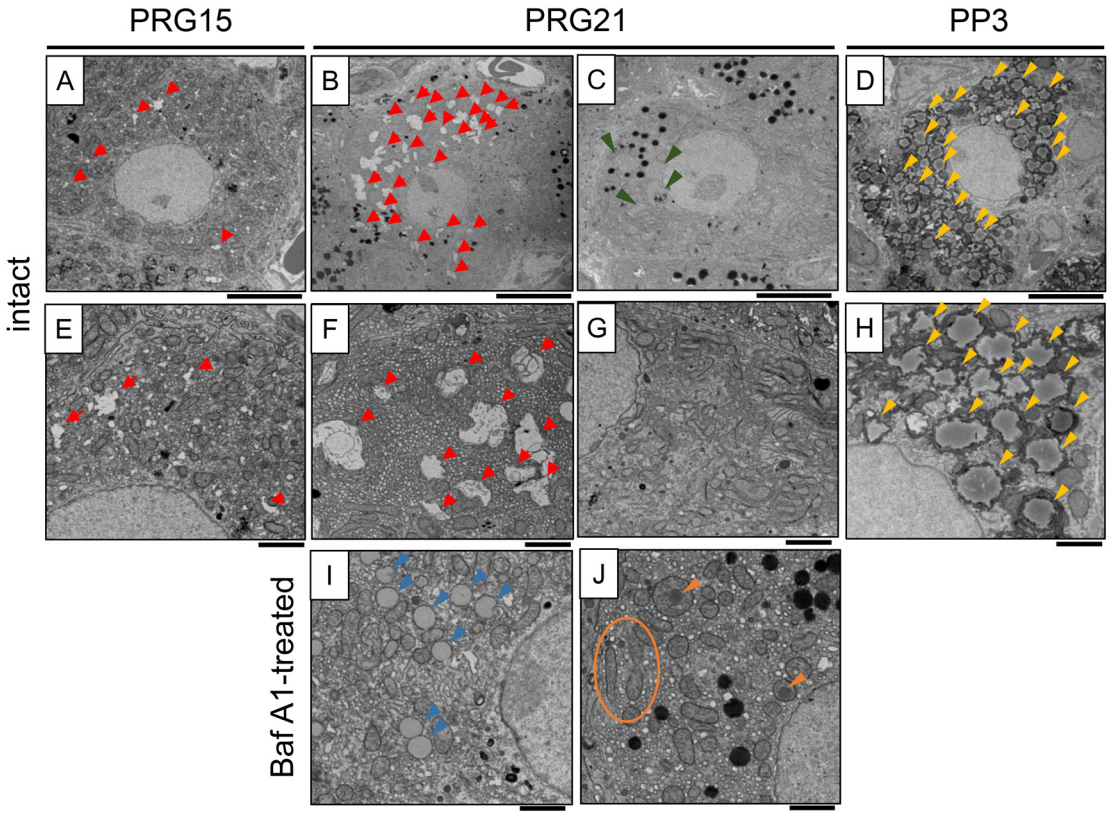

Fig. 3. TEM observation of luteal steroidogenic cells. A, E: PRG15 (intact); B, C, F, G: PRG21 (intact); D, H: PP3 (intact); I, J: PRG21 (Bafilomycin A1-treated on PRG15 and sampled on PRG21). Irregular shapes of voids (red arrowheads) were observed on PRG15 and increased on PRG21. Another type of luteal cell with few voids and a developed endoplasmic reticulum (green arrowheads) was also observed on PRG21. Luteal cells on PP3 contain increased amounts of lipid droplets (yellow arrowheads). In CL treated with Baf A1 on PRG15, luteal cells with decreased voids, increased lipid droplets (blue arrowheads), and abnormal mitochondrial structures (orange circles and arrowheads) were noted at PRG21. Scale bar, 5 µm (A–D) and 2 µm (E–J).

PRG21 but diminished on PP0, and that capillary endothelial cells were predominantly positive on PP0 (Fig. 4D).

Effects of Baf A1 on dam's parturition and fetal growth

As autophagic activity in the CL was augmented from PRG15, we tested the effect of chemical inhibition of autophagy in the ovary on dam parturition and fetal/neonatal growth. Intact rats in our breeding colony deliver neonates very mostly in the morning of PRG23 (72.5%) and less frequently in the evening of PRG22 (23.6%) (Table 1). Rats treated with vehicle on PRG15 showed a subtle delay in delivery, which might be due to the general effects of anesthesia, surgical operation, and also the unusual conditions after treatment. Rats treated with a lower dose of Baf A1 on PRG15 showed variable timing of parturition. Rats treated with the higher dose showed disruption of birth timing. The rate of parturition occurrence in the afternoon of PRG22 was increased (32% *vs*. 5.3% in control and 23.6% in intact group). On the other hand, animals with severely delayed delivery (after the morning of PRG24) were also increased in the high Baf A1 group when compared with the control and intact groups (24% *vs*. 10.5% and 1.1%, respectively). The delivery timing-perturbing effect of Baf A1 was diminished when its administration was delayed by PRG19.

Fetal growth was impaired by both Baf A1-independent and -dependent effects. The litter size was not significantly different among the groups (Table 2); however, the dams that had delayed parturition after Baf A1 treatment tended to have a smaller litter size and some intrauterine fetal death, which were found in the autopsy. In rats treated with a higher dose of Baf A1 at PRG15, body weight of neonates was significantly lower (5.4% reduction) than that of vehicle-treated and intact animals. Fetal body weights, evaluated on PRG18 and PRG21, of vehicle-treated dams were lower than those of the intact dams. This Baf A1-independent reduction was probably due to maternal behavioral and humoral alterations caused by the surgical treatment, including anesthesia. The fetal weight did not differ between the vehicle- and Baf A1-treated groups at any of the time points tested.

Effects of Baf A1 on luteal cell size and P4 secretion

Given the appreciable effects of Baf A1 on maternal and neonatal phenotypes *in vivo*, its effects on CL morphology and function were explored. As it was difficult to use CL tissue weight as a structural index, luteal cell size was evaluated based on the cross-sectional area of the tissue slide. Vehicle treatment on PRG15 did not alter the index on PRG18 (72 h later) compared to that in intact animals, and lower and higher doses of Baf A1 decreased the size to 92.0% and 89.6%, respectively ($P < 0.05$, *vs*. control group) (Fig. 5A). The immunoreactivity for LC3 in Baf A1-treated CL was more intense than that in vehicle-treated CL (data not shown). The Baf A1 treatment on PRG19 also caused a significant reduction in cell size (92.1% of vehicle control group) 2 days later (Fig. 5A).

We subsequently examined whether P4 secretion was altered in rats with disrupted timing of delivery following high-dose Baf A1

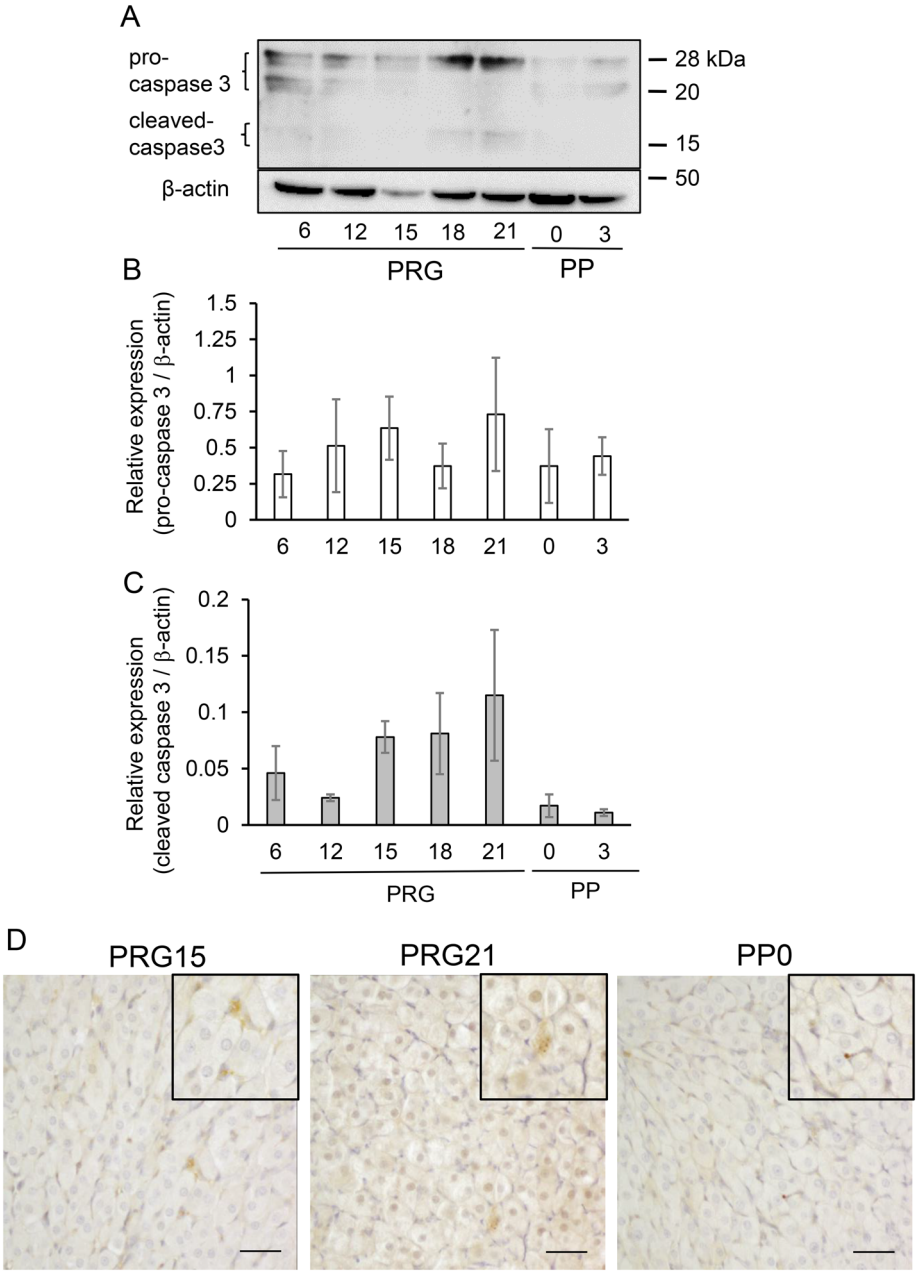

Fig. 4. Expression of caspase 3 protein in CL tissue. (A) Typical immunoblots of caspase 3 in CL tissue throughout pregnancy and postpartum. Protein expression of pro-caspase 3 (B) and cleaved caspase 3 (C) relative to β-actin was determined and shown (mean ± SEM, n = 3). (D) Immunostaining of cleaved caspase 3 in CL. Note the enhanced positive reaction in luteal cells on PRG21 when compared to those on PRG15 and PP0. Scale bar, 50 μm.

treatment of PRG15. P4 levels in each individual at 0, 24, and 72 h after Baf A1 or vehicle treatment were quantified and analyzed in relation to the timing of parturition (divided into three groups of Baf A1-treated rats: the evening of PRG22, in the morning of PRG23 and after the evening of PRG23) (Fig. 5B). The control group showed a gradual, but insignificant, decline in P4 levels. In rats with early delivery (completed by the evening of PRG22), the P4 levels were also lower but not significantly different from those in the control group. P4 levels in Baf A1-treated rats with normal delivery timing (morning of PRG23) were similar to those of the control group. In rats with delayed delivery (after the evening of PRG23), P4 levels were maintained or increased 72 h later, and were significantly higher than those in the control group (Fig. 5B). The varied timing of delivery in Baf A1-treated rats was largely ascribed to the altered dynamics of circulating P4.

Discussion

Comprehensive measurements of autophagic activity (LC3-II/-I ratio), tissue weight of the CL, and blood P4 levels throughout pregnancy and the postpartum period have revealed a positive correlation between autophagy and tissue growth, rather than P4 production. Enhanced autophagy in luteal cells during late pregnancy is supported by immunoreactive LC3 aggregates and abundant multi-membranous microstructures in the cytoplasm. Its increased activity is also linked to the expression of the primary effector of

Table 1. Effect of bafilomycin A1 on the timing of delivery

Day of treatment	Group / Drug	PRG22 am	PRG22 pm	PRG23 am	PRG23 pm	PRG24 am	PRG24 pm	No delivery
Intact		2	42	129	3	2	0	0
PRG15	vehicle	0	1	13	3	1	0	1
	Baf A1 125 pg	2	1	2	1	0	0	1
	Baf A1 625 pg	0	6	8	0	3	0	0
PRG19	vehicle	0	0	0	3	0	0	0
	Baf A1 125 pg	0	0	4	3	0	0	0
	Baf A1 625 pg	0	1	4	0	0	0	0

For PRG15 or PRG19, mother rats were administered a single dose (200 µl/ovary) of bafilomycin A1 (Baf A1, 62.5 or 312.5 pg/ovary, in total 125 or 625 pg/rat) or vehicle intraovarian-bursally, and were examined for the timing of delivery from PRG22 through PRG25 at 0900 h or 1800 h each day. Data from intact rats were obtained from ordinary breeding of laboratory rats over the last several years.

Table 2. Effect of bafilomycin A1 on the fetal / neonatal development

	Body weight (g)			Littersize
	Fetus		Neonate	Neonate
	(PRG18)	(PRG21)	(PRG22–24)	(PRG22–24)
Intact	0.87 ± 0.01 [a]	3.70 ± 0.05 [a]	5.66 ± 0.06 [a]	11.4 ± 0.9
Vehicle	0.79 ± 0.02 [b]	3.52 ± 0.03 [b]	5.64 ± 0.06 [a]	10.5 ± 1.2
Baf A1 625 pg	0.79 ± 0.02 [b]	3.47 ± 0.04 [b]	5.34 ± 0.07 [b]	10.3 ± 1.3

Intact mother rats and rats treated with Baf A1 (625 pg/rat) or vehicle on PRG15 were euthanized on PRG18 or PRG21 or left until delivery. The fetal body weight, neonatal weight, and litter size were also determined. Data are mean ± SEM (n = 15–120 in body weight, n = 12 in litter size). Different letters within the same column indicate significant differences ($P < 0.05$).

apoptosis. Our functional investigation *in vivo* suggests that autophagy contributes to the increase in luteal cell size, influencing P4 secretion, and consequently affecting the timing of delivery and fetal growth. Our data in a pregnant rat model revealed a novel implication of autophagy in CL tissue growth, aligning with the luteotropic effect of beclin 1-mediated autophagy demonstrated in a gene knockout mouse study [20] and histologically suggested by non-experimental animal models (pigs and humans) [16, 21].

Our morphological and functional data strongly suggest that autophagy is active and increases luteal steroidogenic cell size, at least from PRG15 to PRG21. CL tissue growth in pregnant rats is attributed to increased cell size rather than cellular proliferation, with hypertrophy and enhanced protein synthesis promoted by E2 and insulin-like growth factor 1, mediating the PL-II effect [4, 6]. PL-II, E2, and P4, which are established regulators of the rat CL in mid- and late pregnancy, emerge as potential candidates for enhancing autophagy. Recent studies have identified extracellular and intracellular regulators of autophagy in CL, including prostaglandin $F_2\alpha$ [11, 12, 38], extracellular signal-regulated kinase 1/2 [12], hypoxia-inducible factor 1α / bcl-2 interacting protein 3 pathway [13, 19] and AMP-activated protein kinase [2, 38], luteinizing hormone [2, 38], protein kinase A [38] and Akt/mammalian target of rapamycin signaling [2, 19]. These findings were obtained from studies on regressing CL and are therefore fragmentary. Although we did not identify an enhancer or suppressor of autophagy in our experimental model, it is reasonable to consider that the homeostatic action of autophagy contributes to luteal cell hypertrophy to maintain pregnancy. The study with ovarian-specific beclin 1-deficient mice emphasized an essential role of autophagy in sustained P4 secretion during mid-pregnancy, but lacked information on the structural indices of CL tissues [20].

The effect of autophagy on P4 secretory function in the pregnant CL appears to be complex. When compared to the tissue weight of the CL, autophagic activity is temporally less associated with the secretion of P4 or total progestins [39, 40]. In addition, a single local administration of Baf A1 caused varied P4 secretory responses (inhibition and maintenance), resulting in varied timing of parturition. Considering the similarity of the characteristic features of autophagy itself as a double-edged sword controlling cellular survival or death [7, 8] and of CL progestational activity under opposite regulation, which determines the maintenance or termination of pregnancy in many animal species [1, 2], autophagy may be deeply implicated in CL regulation. Perturbation of P4 alteration and the timing of delivery after autophagy inhibition might be evidence for the autophagy-mediated modulation of fine-tuned P4 production. One research group, employing the previously reported method in order to study uterine autophagy in mice *in vivo* [41], used systemic (intraperitoneal) and chronic (five time-repeated) treatments with other autophagy inhibitors, 3-methyladenine and chloroquine, to study the impact of CL autophagy in pregnant rats *in vivo* [14]. They showed a significant reduction in serum P4 levels during mid-pregnancy (PRG16), but not early (PRG10) or late (PRG21) pregnancy, claiming that autophagic activity in the CL augments P4 secretion only during mid-pregnancy. Curiously, they provided no description of maternal parturition and fetal and neonatal growth, and did not discuss the effects of inhibitors on extra-ovarian organs [14]. Autophagy occurs in multiple gestation-associated organs whose mutual regulation in endocrine and paracrine modes is crucial for normal maternal pregnancy and fetal growth [42–44]. The systemic

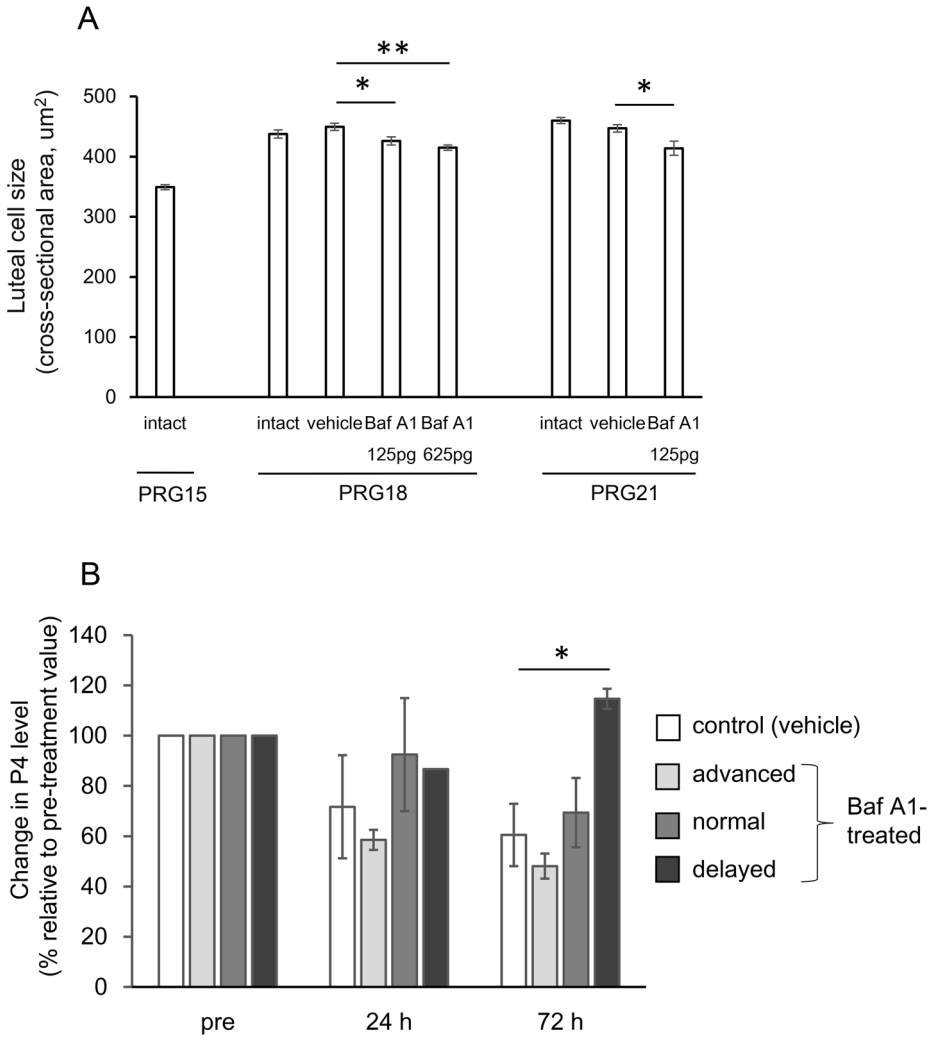

Fig. 5. Effects of bafilomycin A1 on luteal cell size and P4 secretory function. (A) On PRG15, mother rats were administered with a single dose of bafilomycin A1 (Baf A1, 125 or 625 pg/rat) or vehicle intraovarian-bursally and were examined for luteal cell size in the ovarian tissue sampled on PRG18. Other rats were done with vehicle or Baf A1 (125 pg/rat) on PRG19 and were examined as well on PRG21. Cell size of luteal cells randomly selected (30 cells/CL, 3 CL/rat, ≥ 3 rats in each group) were quantitatively analyzed using Image J software and expressed as mean ± SEM. * $P < 0.05$, ** $P < 0.01$. (B) Rats treated with vehicle or Baf A1 (625 pg/rat) on PRG15 had blood taken at 0, 24, and 72 h after the drug challenge and were measured for their timing of parturition. Baf A1-treated dams were divided into three groups of delivery timing (advanced, before and in the evening of PRG22; normal, in the morning of PRG23; delayed, in and after the evening of PRG23). P4 levels in their circulating blood, relative to each on PRG15, are expressed as mean ± SEM (n = 9, the control group; n = 3–5, experimental groups). * $P < 0.05$.

administration of autophagy modulators is inadequate for dissecting and also selectively evaluating the functional role of autophagy in a given organ within the context of reproduction [45]. In addition, our dose of Baf A1 was much lower than that systemically administered in order to demonstrate its protective effect in a mouse model of myocardial infarction (0.3 mg/kg) [46]. Our *in vivo* experimental design was aimed at limiting the action of the inhibitor to a relatively specific site and period, making it more appropriate to evaluate its direct and primary effects on the CL and the systemic and secondary effects resulting from altered CL function. The inhibitory effect of Baf A1 on autophagy was partly confirmed morphologically. The mechanistic pathway of aberrant P4 production and impaired fetal development following Baf A1 treatment remains unclear. The former can be a possible cause of the latter, because altered metabolism and circulation of P4 in dams and fetuses are associated with intra-uterine growth restriction or perinatal death in rodents [47–49]. The normal progression of CL activity supported by autophagy *in situ* is critical for the proper timing of gestational termination and parturition induction and intact neonatal birth.

Recent advancement in autophagy research has implicated autophagy and its subsets, lipophagy and mitophagy, in steroidogenesis across various tissue types [7, 22]. Lipophagy specifically targets LD, a potential source of cholesterol esters, whereas mitophagy targets mitochondria, where free cholesterol is transported and metabolized to pregnenolone [7, 22]. The mobilization of cholesterol from intracellular pools or extracellular sources appears to be controlled by autophagy, as demonstrated by ecdyson production in the Drosophila prothoracic gland [50], testosterone production in murine Leydig cells [51], and E2 and P4 production in isolated human ovarian tissue [52]. Gawriluk *et al.* claimed that beclin 1-mediated LD formation in murine luteal cells is critical for adequate P4 production during mid-pregnancy [20]. Conversely, several EM studies have shown that LD content in luteal cells is inversely related to P4 production in pregnant rats [23–26]. A very recent study with mCherry-HPos

mice revealed that LDs in CL were massively degraded via lipolysis rather than lipophagy in early and mid-pregnancy and accumulated around the time of parturition [53]. Our finding from TEM and histochemical studies is that LD content was increased in late pregnancy and postpartum and could be affected by autophagic activity. Accumulated evidence from pregnant rat models has shown that the source of cholesterol is luteal endogenous cholesterol in the first half of pregnancy and the uptake and degradation of circulating high- and low-density lipoproteins in the latter half [3, 54]. The dependence of P4 production on LDs likely varies with gestational time. Autophagic degradation of mitochondria, as shown in our observation, may affect one of critical steps of steroidogenesis. Autophagy regulation of steroidogenesis is well conserved across animal species and tissue types, but its molecular and subcellular mechanisms, involving autophagy (macroautophagy, lipophagy and mitophagy) and LDs availability, appear highly variable and complex [22].

Whether autophagy causes survival or death and whether autophagy/ACD interacts with apoptosis are important issues regarding tissue and cell homeostasis [7–9]. The rat CL of pregnancy is an excellent model for investigating these issues. The temporal alteration in active caspase-3 levels in pregnant rats was consistent with that of a previous report [28] but differed from that in pseudopregnant rats [11]. Choi *et al*. showed that luteal expression of both LC3-II and cleaved caspase 3 in a gonadotropin-primed immature pseudopregnant rat model increased progressively until day 20 but failed to relate them to functional and structural demise [11]. In contrast, our findings showed similar alterations in autophagic and apoptotic indices and their association with functional rather than structural luteolysis. As claimed previously, rat CL of pregnancy did not elicit degenerating features, such as the typical apoptotic phenotype of DNA fragmentation in luteal cells and multiple focal occurrences of inflammatory-like responses that were observed in the regressing CL of pseudopregnancy and cycling [29, 55]. Our current hypothesis is that elevated autophagic activity may inhibit the caspase 3-dependent pathway and apoptosis induction in luteal cells of pregnant rats. Choi *et al*. further demonstrated *in vitro* that 3-methyladenine and Baf A1 inhibited and promoted apoptosis, respectively, through the up-regulation of bcl2 or BAX [11]. Our perturbation experiments were performed starting from PRG15 and PRG19. Thus, the functional role of autophagy may change from cytoprotective to cytotoxic over time. Accumulating evidence supports that ACD occurs in a variety of types and species of regressing CL [9, 10]. In the structurally regressing CL of peri-parturient rats with reduced levels of LC3-II and cleaved caspase 3, the possible interplay of autophagy, ACD, and apoptosis in structural demise warrants further investigation.

In conclusion, our study provides the first evidence of a close association between autophagy and CL tissue growth throughout pregnancy in mammals. Autophagic activity in the CL of pregnant rats contributes to luteal cell hypertrophy, potentially affecting P4 secretion and parturition timing. These findings shed light on the multifaceted regulatory mechanism of the CL, where autophagy may play multiple roles in regulating cellular size, affecting P4 production, and the duration of pregnancy in species that rely solely on the CL as a P4 source.

Conflict of interests: The authors declare that there is no conflict of interest.

Acknowledgments

The authors thank H. Yoshio and Y. Hidaka for their assistance with the experiments. This work was supported in part by a special grant from MEXT, Japan for the promotion of cooperative research by Kitasato University and Iwate University.

References

1. **Stocco C, Telleria C, Gibori G.** The molecular control of corpus luteum formation, function, and regression. *Endocr Rev* 2007; **28**: 117–149. [Medline] [CrossRef]
2. **Przygrodzka E, Plewes MR, Davis JS.** Luteinizing hormone regulation of inter-organelle communication and fate of the corpus luteum. *Int J Mol Sci* 2021; **22**: 9972. [Medline] [CrossRef]
3. **Gibori G.** The corpus luteum of pregnancy. *In*: Adashi EY, Leung PCK (eds.), The Ovary. New York: Raven Press; 1993: 261–317.
4. **Bowen-Shauver JM, Gibori G.** The corpus luteum of pregnancy. *In* Adashi EY, Leung PCK (eds.), The Ovary. San Diego: Elsevier Academic Press; 2003: 201–230.
5. **Shiota K, Furuyama N, Takahashi M.** Placental lactogen secretion during prolonged-pregnancy in the rat: the ovary plays a pivotal role in the control of placental function. *Endocrinol Jpn* 1991; **38**: 541–549. [Medline] [CrossRef]
6. **Gibori G, Keyes PL.** Role of intraluteal estrogen in the regulation of the rat corpus luteum during pregnancy. *Endocrinology* 1978; **102**: 1176–1182. [Medline] [CrossRef]
7. **Mizushima N, Komatsu M.** Autophagy: renovation of cells and tissues. *Cell* 2011; **147**: 728–741. [Medline] [CrossRef]
8. **Gordy C, He Y-W.** The crosstalk between autophagy and apoptosis: where does this lead? *Protein Cell* 2012; **3**: 17–27. [Medline] [CrossRef]
9. **Teeli AS, Leszczyński P, Krishnaswamy N, Ogawa H, Tsuchiya M, Śmiech M, Skarzynski D, Taniguchi H.** Possible mechanism for maintenance and regression of corpus luteum through the ubiquitin-proteasome and autophagy system regulated by transcriptional factors. *Front Endocrinol (Lausanne)* 2019; **10**: 748. [Medline] [CrossRef]
10. **Hojo T, Skarzynski DJ, Okuda K.** Apoptosis, autophagic cell death, and necroptosis: different types of programmed cell death in bovine corpus luteum regression. *J Reprod Dev* 2022; **68**: 355–360. [Medline] [CrossRef]
11. **Choi J, Jo M, Lee E, Choi D.** The role of autophagy in corpus luteum regression in the rat. *Biol Reprod* 2011; **85**: 465–472. [Medline] [CrossRef]
12. **Choi J, Jo M, Lee E, Choi D.** ERK1/2 is involved in luteal cell autophagy regulation during corpus luteum regression via an mTOR-independent pathway. *Mol Hum Reprod* 2014; **20**: 972–980. [Medline] [CrossRef]
13. **Tang Z, Chen J, Zhang Z, Bi J, Xu R, Lin Q, Wang Z.** HIF-1α activation promotes luteolysis by enhancing ROS levels in the corpus luteum of pseudopregnant rats. *Oxid Med Cell Longev* 2021; **2021**: 1764929. [Medline] [CrossRef]
14. **Tang Z, Zhang Z, Zhang H, Wang Y, Zhang Y, Zhao J, Yang H, Wang Z.** Autophagy attenuation hampers progesterone synthesis during the development of pregnant corpus luteum. *Cells* 2019; **9**: 71. [Medline] [CrossRef]
15. **Grzesiak M, Knapczyk-Stwora K, Slomczynska M.** Induction of autophagy in the porcine corpus luteum of pregnancy following anti-androgen treatment. *J Physiol Pharmacol* 2016; **67**: 933–942. [Medline]
16. **Grzesiak M, Michalik A, Rak A, Knapczyk-Stwora K, Pieczonka A.** The expression of autophagy-related proteins within the corpus luteum lifespan in pigs. *Domest Anim Endocrinol* 2018; **64**: 9–16. [Medline] [CrossRef]
17. **Wen X, Liu L, Li S, Lin P, Chen H, Zhou D, Tang K, Wang A, Jin Y.** Prostaglandin $F_2\alpha$ induces goat corpus luteum regression via endoplasmic reticulum stress and autophagy. *Front Physiol* 2020; **11**: 868. [Medline] [CrossRef]
18. **Aboelenain M, Kawahara M, Balboula AZ, Montasser Ael-M, Zaabel SM, Okuda K, Takahashi M.** Status of autophagy, lysosomal activity and apoptosis during corpus luteum regression in cattle. *J Reprod Dev* 2015; **61**: 229–236. [Medline] [CrossRef]
19. **Tang Z, Zhang Z, Lin Q, Xu R, Chen J, Wang Y, Zhang Y, Tang Y, Shi C, Liu Y, Yang H, Wang Z.** HIF-1α/BNIP3-mediated autophagy contributes to the luteinization of graluosa cells during the formation of corpus luteum. *Front Cell Dev Biol* 2021; **8**: 619924. [Medline] [CrossRef]
20. **Gawriluk TR, Ko C, Hong X, Christenson LK, Rucker EB 3rd.** Beclin-1 deficiency in the murine ovary results in the reduction of progesterone production to promote preterm labor. *Proc Natl Acad Sci USA* 2014; **111**: E4194–E4203. [Medline] [CrossRef]
21. **Gaytán M, Morales C, Sánchez-Criado JE, Gaytán F.** Immunolocalization of beclin 1, a bcl-2-binding, autophagy-related protein, in the human ovary: possible relation to life span of corpus luteum. *Cell Tissue Res* 2008; **331**: 509–517. [Medline] [CrossRef]
22. **Bassi G, Sidhu SK, Mishra S.** The expanding role of mitochondria, autophagy and lipophagy in steroidogenesis. *Cells* 2021; **10**: 1851. [Medline] [CrossRef]
23. **Enders AC, Lyons WR.** Observations on the fine structure of lutein cells. *J Cell Biol* 1964; **22**: 127–141. [Medline] [CrossRef]
24. **Long JA.** Corpus luteum of pregnancy in the rat—ultrastructural and cytochemical observations. *Biol Reprod* 1973; **8**: 87–99. [Medline] [CrossRef]
25. **Kohsaka T, Niimura S, Ishida K.** Microstructure of granulosa-lutein and theca-lutein cells in pregnant rat (in Japanese). *Niigata Daigaku Nogakubu Kenkyu Hokoku* 1983; **35**: 63–70.
26. **Guraya SS.** Histochemical observations on the lipid changes in the rat corpus luteum during various reproductive states. *J Reprod Fertil* 1975; **42**: 59–65. [Medline] [CrossRef]
27. **Carambula SF, Pru JK, Lynch MP, Matikainen T, Gonçalves PBD, Flavell RA, Tilly**

JL, Rueda BR. Prostaglandin $F_2\alpha$- and FAS-activating antibody-induced regression of the corpus luteum involves caspase-8 and is defective in caspase-3 deficient mice. *Reprod Biol Endocrinol* 2003; **1**: 15. [Medline] [CrossRef]

28. **Peluffo MC, Stouffer RL, Tesone M.** Activity and expression of different members of the caspase family in the rat corpus luteum during pregnancy and postpartum. *Am J Physiol Endocrinol Metab* 2007; **293**: E1215–E1223. [Medline] [CrossRef]
29. **Satoh H, Yoshio H, Kawaminami M, Kurusu S.** Type-dependent differences in Fas expression and phagocytes distribution in rat corpora lutea during natural regression: an immunohistochemical evidence. *J Vet Med Sci* 2017; **78**: 1771–1777. [Medline] [CrossRef]
30. **Kurusu S, Kaizo K, Ibashi M, Kawaminami M, Hashimoto I.** Luteal phospholipase A_2 activity increases during functional and structural luteolysis in pregnant rats. *FEBS Lett* 1999; **454**: 225–228. [Medline] [CrossRef]
31. **Kurusu S, Suzuki K, Taniguchi K, Yonezawa T, Kawaminami M.** Structural regression of the rat corpus luteum of pregnancy: relationship with functional regression, apoptotic cell death, and the suckling stimulus. *Zool Sci* 2009; **26**: 729–734. [Medline] [CrossRef]
32. **Funahashi R, Sakamoto T, Taguchi N, Naiki R, Terashima R, Kawaminami M, Kurusu S.** Possible role of PPARγ in the negative regulation of ovulatory cascade and luteal development in rats. *J Vet Med Sci* 2017; **79**: 1043–1051. [Medline] [CrossRef]
33. **Sugiyama M, Machida N, Yasunaga A, Terai N, Fukasawa H, Ono HK, Kobayashi R, Nishiyama K, Hashimoto O, Kurusu S, Yoshioka K.** Vaginal mucus in mice: developmental and gene expression features of epithelial mucous cells during pregnancy. *Biol Reprod* 2021; **105**: 1272–1282. [Medline] [CrossRef]
34. **Komiya Y, Sugiyama M, Koyama C, Kameshima S, Ochiai M, Adachi Y, Yokoyama I, Fukasawa H, Yoshioka K, Arihara K.** Dietary olive oil intake induces female-specific hepatic lipid accumulation without metabolic impairment in mice. *Nutr Res* 2023; **112**: 11–19. [Medline] [CrossRef]
35. **Kurusu S, Sapirstein A, Bonventre JV.** Group IVA phospholipase A_2 optimizes ovulation and fertilization in rodents through induction of and metabolic coupling with prostaglandin endoperoxide synthase 2. *FASEB J* 2012; **26**: 3800–3810. [Medline] [CrossRef]
36. **Masuda K, Haruta S, Orino K, Kawaminami M, Kurusu S.** Autotaxin as a novel, tissue-remodeling-related factor in regressing corpora lutea of cycling rats. *FEBS J* 2013; **280**: 6600–6612. [Medline] [CrossRef]
37. **Yoshii SR, Mizushima N.** Monitoring and measuring autophagy. *Int J Mol Sci* 2017; **18**: 1865. [Medline] [CrossRef]
38. **Przygrodzka E, Monaco CF, Plewes MR, Li G, Wood JR, Cupp AS, Davis JS.** Protein kinase A and 5′ AMP-activated protein kinase signaling pathways exert opposite effects on induction of autophagy in luteal cells. *Front Cell Dev Biol* 2021; **9**: 723563. [Medline] [CrossRef]
39. **Hashimoto I, Henricks DM, Anderson LL, Melampy RM.** Progesterone and pregn-4-en-20 α-ol-3-one in ovarian venous blood during various reproductive states in the rat. *Endocrinology* 1968; **82**: 333–341. [Medline] [CrossRef]
40. **Uchida K, Kadowaki M, Nomura Y, Miyata K, Miyake T.** Relationship between ovarian progestin secretion and corpora lutea function in pregnant rats. *Endocrinol Jpn* 1970; **17**: 499–507. [Medline] [CrossRef]
41. **Choi S, Shin H, Song H, Lim HJ.** Suppression of autophagic activation in the mouse uterus by estrogen and progesterone. *J Endocrinol* 2014; **221**: 39–50. [Medline] [CrossRef]
42. **de Andrade Ramos BR, Witkin SS.** The influence of oxidative stress and autophagy cross regulation on pregnancy outcome. *Cell Stress Chaperones* 2016; **21**: 755–762. [Medline] [CrossRef]
43. **Cao B, Camden AJ, Parnell LA, Mysorekar IU.** Autophagy regulation of physiological and pathological processes in the female reproductive tract. *Am J Reprod Immunol* 2017; **77**: e12650. [Medline] [CrossRef]
44. **Liu C, Wu B, Liu W, Li W.** Role of autophagy in male and female fertility. *Curr Opin Physiol* 2022; **30**: 100611. [CrossRef]
45. **Moulis M, Vindis C.** Methods for measuring autophagy in mice. *Cells* 2017; **6**: 14. [Medline] [CrossRef]
46. **Kanamori H, Takemura G, Goto K, Maruyama R, Ono K, Nagao K, Tsujimoto A, Ogino A, Takeyama T, Kawaguchi T, Watanabe T, Kawasaki M, Fujiwara T, Fujiwara H, Seishima M, Minatoguchi S.** Autophagy limits acute myocardial infarction induced by permanent coronary artery occlusion. *Am J Physiol Heart Circ Physiol* 2011; **300**: H2261–H2271. [Medline] [CrossRef]
47. **Clarke CL, Sutherland RL.** Progestin regulation of cellular proliferation. *Endocr Rev* 1990; **11**: 266–301. [Medline] [CrossRef]
48. **Ishida M, Choi JH, Hirabayashi K, Matsuwaki T, Suzuki M, Yamanouchi K, Horai R, Sudo K, Iwakura Y, Nishihara M.** Reproductive phenotypes in mice with targeted disruption of the 20α-hydroxysteroid dehydrogenase gene. *J Reprod Dev* 2007; **53**: 499–508. [Medline] [CrossRef]
49. **Baud O, Berkane N.** Hormonal changes associated with intra-uterine growth restriction: Impact on the developing brain and future neurodevelopment. *Front Endocrinol (Lausanne)* 2019; **10**: 179. [Medline] [CrossRef]
50. **Texada MJ, Malita A, Christensen CF, Dall KB, Faergeman NJ, Nagy S, Halberg KA, Rewitz K.** Autophagy-mediated cholesterol trafficking controls steroid production. *Dev Cell* 2019; **48**: 659–671.e4. [Medline] [CrossRef]
51. **Gao F, Li G, Liu C, Gao H, Wang H, Liu W, Chen M, Shang Y, Wang L, Shi J, Xia W, Jiao J, Gao F, Li J, Chen L, Li W.** Autophagy regulates testosterone synthesis by facilitating cholesterol uptake in Leydig cells. *J Cell Biol* 2018; **217**: 2103–2119. [Medline] [CrossRef]
52. **Esmaeilian Y, Hela F, Bildik G, İltumur E, Yusufoglu S, Yildiz CS, Yakin K, Kordan Y, Oktem O.** Autophagy regulates sex steroid hormone synthesis through lysosomal degradation of lipid droplets in human ovary and testis. *Cell Death Dis* 2023; **14**: 342. [Medline] [CrossRef]
53. **Mitsui J, Ibayashi M, Aizawa R, Ishikawa T, Miyasaka N, Tsukamoto S.** Lipid droplets synthesized during luteinization are degraded after pregnancy. *J Reprod Dev* 2024; **70**: 72–81. [Medline] [CrossRef]
54. **Azhar S, Khan I, Puryear T, Chen YD, Gibori G.** Luteal cell 3-hydroxy-3-methylglutaryl coenzyme-A reductase activity and cholesterol metabolism throughout pregnancy in the rat. *Endocrinology* 1988; **123**: 1495–1503. [Medline] [CrossRef]
55. **Goyeneche AA, Martinez IL, Deis RP, Gibori G, Telleria CM.** In vivo hormonal environment leads to differential susceptibility of the corpus luteum to apoptosis in vitro. *Biol Reprod* 2003; **68**: 2322–2330. [Medline] [CrossRef]